Using Mechanical Reliability in Multiobjective Optimal Meter Placement for Pipe Burst Detection

Donghwi Jung, Ph.D.[1]; and Joong Hoon Kim, Ph.D., P.E.[2]

Abstract: A multiobjective optimal meter placement (MOMP) model is proposed for water distribution system (WDS) pipe burst detection to (1) minimize the normalized total meter cost, (2) maximize the detection probability, (3) minimize the rate of false alarms, and (4) maximize the meter network's mechanical reliability. The mechanical reliability is a meter network's ability to continuously provide informative data/measurement even under measurement failures originating from either missing measurements for time steps or meter malfunction. A novel method for quantifying mechanical reliability is developed based on the simulation of a single-meter failure. In addition to meter locations, the optimal ratio between the pressure and pipe flow meters was identified for a predefined number of meters. The proposed MOMP model was demonstrated on two networks from the literature with different configurations, characteristics, and numbers of components. The results suggest that the proposed MOMP model should be used to determine the optimal meter location and best set of meters for high detectability and mechanical reliability of a specific network of interest. **DOI: 10.1061/(ASCE)WR.1943-5452.0000953.** © *2018 American Society of Civil Engineers.*

Introduction

Various system variables, such as the pressure, pipe flow, and customer demand, are measured by meters installed in a water distribution system (WDS). Useful information for system operation and management is extracted from the data collected at meters and sent to a supervisory control and data acquisition (SCADA) system. In order to maximize the information gained from the meter data, effective informatics techniques need to be used (Abbott 1999), and meters of a suitable type should be installed at optimal locations (Bragalli et al. 2016; Jung and Kim 2017). This study focuses on the latter consideration.

During the last two decades, optimal meter placement (OMP) has been one of the most popular problems in the WDS research domain and has been tackled for different purposes: (1) state estimation (Kang and Lansey 2010; Bragalli et al. 2016; Jung and Kim 2017), (2) leakage/pipe burst detection and identification (Pérez et al. 2009; Farley et al. 2010; Huang et al. 2012; Zheng and Yuan 2012; Hagos et al. 2016; Steffelbauer and Fuchs-Hanusch 2016; Sela Perelman et al. 2016), (3) contamination detection (e.g., Sankary and Ostfeld 2017), and (4) model calibration (Kapelan et al. 2003, 2005; Simone et al. 2016). Different types of meters have been confirmed to be more efficient than others for different problems. Generally, most OMP approaches to leakage/pipe burst detection have been based on pressure meter data and a sensitivity matrix (e.g., Jacobian matrix) (e.g., Farley et al. 2010), whereas those for demand estimation (DE) use pipe flow data (e.g., Jung and Kim 2017).

This study is the first to introduce meter network reliability (i.e., sampling network reliability) to the WDS OMP problem. A meter network is defined as a group of meters spatially distributed throughout a WDS. Meter network reliability is defined as a meter network's ability to provide useful data (e.g., pressure, pipe flow, and customer demand) for various WDS operational and management purposes (e.g., leakage/pipe burst detection) with acceptable accuracy and precision and without missing data. Therefore, meter network reliability consists of (1) performance reliability, and (2) mechanical reliability. The former refers to a meter network's capability to reliably observe the system variables as close as possible to their true values, whereas the latter is defined as the ability to continuously provide informative data/measurements even in the event of measurement failures originating from missing time-step measurements or meter malfunction. Performance reliability is often estimated with and affected by data analysis methods used with a meter network. For example, a coupled model consisting of a meter network and demand forecasting submodule with high accuracy [e.g., root-mean square error (RMSE)] and low uncertainty (e.g., narrow confidence interval) has high performance reliability. Mechanical reliability is high if informative data can still be provided even if one of the meters malfunctions (i.e., no data are sent from the failed meter).

Many studies have been devoted to considering the concept of performance reliability for the WDS OMP problem. Kang and Lansey (2010) proposed an OMP methodology for WDS DE with three objectives: minimize nodal DE uncertainty, minimize nodal pressure prediction uncertainty, and minimize the absolute error of the DE. Jung and Kim (2017) introduced an optimal node grouping and meter placement method for WDS DE to minimize the RMSE of the DE. The number of meters was defined before optimization in the aforementioned two studies. Securing a high level for this class of reliability fits well to the original goal of the OMP problem.

However, to the best of the authors' knowledge, no study has incorporated the mechanical reliability of a meter network into the WDS OMP problem. Most studies solved each OMP problem under the assumption that all meters successfully function. However, meter data are often not received by the SCADA in reality because of mechanical failure of a meter or communication system

[1]Dept. of Civil Engineering, Keimyung Univ., 1095 Dalgubeol-daero, Dalseo-gu, Daegu 42601, South Korea. Email: donghwiku@gmail.com

[2]School of Civil, Environmental and Architectural Engineering, Korea Univ., Anam-ro 145, Seongbuk-gu, Seoul 02841, South Korea (corresponding author). Email: jaykim@korea.ac.kr

Note. This manuscript was submitted on August 27, 2017; approved on January 19, 2018; published online on May 9, 2018. Discussion period open until October 9, 2018; separate discussions must be submitted for individual papers. This paper is part of the ***Journal of Water Resources Planning and Management***, © ASCE, ISSN 0733-9496.

issues. This is becoming common for hyperconnected systems vulnerable to cyberattacks (Taormina and Galelli 2017; Taormina et al. 2017). High performance reliability cannot be achieved without an acceptable level of mechanical reliability. Therefore, the mechanical reliability of a meter network should be considered for an OMP problem.

In a real network, a set of pipe flow and pressure meters is located at critical points. For example, pipe flow meters are generally positioned at the inlet pipe of each district metering area, and pressure meters are around pressure-reducing valve stations or pump stations. However, few OMP studies have considered different types of meters (e.g., pressure and pipe flow meters) simultaneously. Sankary and Ostfeld (2017) proposed a mobile senor placement approach for contamination event detection to identify the tradeoff relationships among the population affected prior to detection, detection time, and meter cost. They considered two types of sensors: fixed and mobile. They used normalized costs for the two sensors to calculate the total system metering cost.

In the present study, an OMP methodology was developed for WDS pipe burst detection that considers mechanical reliability. The proposed method is a multiobjective OMP (MOMP) model that minimizes the total meter cost, maximizes detectability [i.e., maximizes detection probability (DP) and minimizes the rate of false alarms (RF)], and maximizes the meter network's mechanical reliability. A novel mechanical reliability quantification method was developed based on the simulation of a single-meter failure. Either the pipe flow or pressure meter can be selected and located at a meter location with a predefined total number of meters (*nmeter*). The total meter cost is computed based on the normalized cost of the two meters. The proposed method was demonstrated on the Austin (Brion and Mays Mays 1991) and Balerma (Reca and Martínez 2006) networks with different configurations, characteristics, and numbers of components.

Methodology

In this section, the detectability measures used in this study are described first, followed by the proposed meter mechanical reliability quantification method. Finally, the normalization method for the meter cost and an overview and details of the proposed MOMP model are presented.

Detectability Measures

WDS pipe burst detectability consists of detection effectiveness and efficiency. The detection effectiveness refers to how well burst events are detected and false alarms are avoided with natural random patterns (Medhanie et al. 2016). The former is measured by DP, and the latter is measured by RF. DP is the ratio of burst events that are detected (*ndetbevent*) to the total number of burst events (*ntotbevent*)

$$\mathrm{DP} = \frac{ndetevent}{ntotevent} \tag{1}$$

RF is the proportion of natural random events in which a false alarm is issued to the total number of natural events. DP is a Type II error (i.e., false negative) index, whereas RF is a Type I error (i.e., false positive) index. Burst events are pipe bursts that occur at different locations and initiation times with different magnitudes. Pressure and pipe flow measurements obtained under the failure condition are provided to a detection method to calculate DP. In this study, a burst that was not detected within 48 h of its initiation was assumed to be a nondetected event. For the calculation of RF, pipe bursts are not considered, only the randomness in demand. A natural random event is a normal random system condition in a 48-h period during which measurements are provided to calculate RF. For example, if a certain detection method issues an alarm for 80 events out of a total 100 burst events, DP is calculated to be 80%. On the other hand, if a method issues an alarm for two natural random events out of a total 100 natural events for which no alarm should be issued, the RF is 2%.

Therefore, a meter network with a high DP and low RF is favored with respect to network reliability and robustness. Hagos et al. (2016) proposed a binary integer programming model to optimize the meter location for WDS pipe burst detection by maximizing DP given a predefined level of RF as a constraint. For more details on DP and RF, please refer to the studies by Jung et al. (2015) and Jung and Lansey (2015).

Detection efficiency refers to the rapidity of detection. The average detection time (ADT) is defined as the averaged value of the time for detection and can be considered in an OMP problem as an additional detection efficiency measure to the aforementioned two detection effectiveness measures. If DP and RF are equal for two networks, the one with a shorter ADT is preferred. Increasing DP indirectly decreases ADT because the detection time for a nondetected event is infinite (∞). Therefore, the two effectiveness measures of DP and RF are optimized by the proposed MOMP model.

Mechanical Reliability of a Meter Network

In this study, a meter network's mechanical reliability was defined as the network's ability to provide useful information for a WDS pipe burst detection even in the event of meter failure. Therefore, the reliability and robustness of a meter network are quantified based on a meter failure simulation. Because the simultaneous failure of multiple meters is of low likelihood, only single-meter failures were considered to assess the mechanical reliability. In this study, the coefficient of variation (CV) of DP in the event of meter failure was used as a mechanical reliability indicator.

Fig. 1 shows a flowchart for calculating the mechanical reliability index. For a given meter set with a total number of meters N (i.e., a set of integer values indicating N meter locations), one of

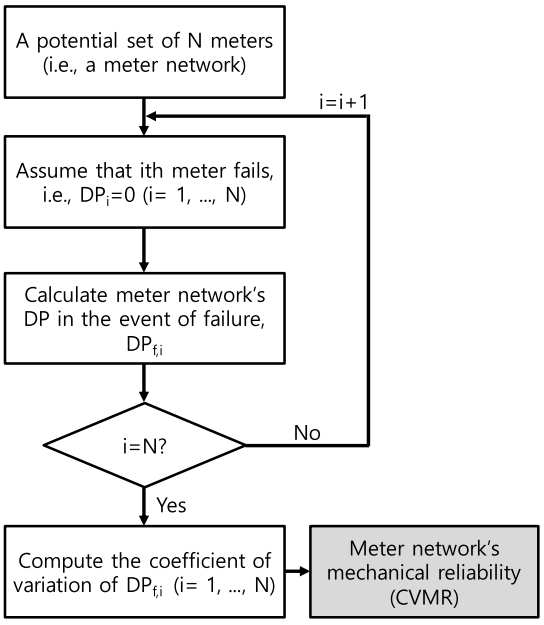

Fig. 1. Procedure to calculate the mechanical reliability of a meter network.

the meters (ith meter, $i = 1, \ldots, N$) is assumed to not send any data to SCADA. This represents a meter failure originating from meter malfunction and communication system failure. Thus, the ith meter's DP (DP_i) is set to zero. The partially impaired meter network's DP in the event of failure of the ith meter ($DP_{f,i}$) is then computed, in which the detection of each burst is determined based on an individual meter's detection of the burst in the meter network excluding the failed meter. The failed/impaired meter is then assumed to return to its normal condition, and another one fails; the preceding calculations are repeated until the failure of all meters has been evaluated (i.e., $DP_{f,i}$ is calculated for $i = 1, \ldots, N$).

The CV of $DP_{f,i}$ (CVMR) is then calculated

$$\text{CVMR} = \frac{\sigma(\text{DP}_{f,i})}{\text{avg}(\text{DP}_{f,i})}, \qquad i = 1, \ldots, N \tag{2}$$

where $\text{avg}(\text{DP}_{f,i})$ and $\sigma(\text{DP}_{f,i})$ = average and standard deviation, respectively, of $DP_{f,i}$ ($i = 1, \ldots, N$). A high mechanical reliability is indicated by a low CVMR. Therefore, a meter network with a low CVMR is preferred because this indicates a high expected DP in the event of a single-meter failure [denominator in Eq. (2)] and low variation in the detection performance in the event of failure [numerator in Eq. (2)].

Similar processes based on single-meter failures can be implemented to quantify the mechanical reliability of a meter network for other purposes. For example, an estimation accuracy indicator (e.g., RMSE) can be used instead of DP to assess the mechanical reliability for WDS demand estimation. In this study, each meter was assumed to have the same failure probability with identical properties (e.g., meter age, battery, and maintenance conditions), which should hold true especially for small- and medium-size networks. A Monte Carlo simulation can be used for a meter network with different meter conditions (e.g., different types of meters).

Meter Network Cost

Generally, a pipe flow meter is more expensive to install than a pressure meter because of the high installation cost. The ground is trenched and excavated; then, part of the pipe wall should be cut off. With the addition of backfill and compaction, such groundwork generates high costs and, in some cases, social costs due to utility interference and traffic control. On the other hand, a pressure meter (e.g., piezometer) can be placed on a hydrant without the need for such groundwork.

Other groups have confirmed that pressure data are more informative for pipe burst detection than pipe flow data (Jung et al. 2015; Hagos et al. 2016). Although most previous OMP studies considered pressure meters because of this meter type's availability and easy implementation (Farley et al. 2010), Hagos et al. (2016) identified a potential benefit of considering not only pressure meters but also pipe flow meters; they found that (1) pressure meters detect common burst events, and pipe flow meters detect different unique events; and (2) DP of a pressure meter is higher than that of a pipe flow meter. Therefore, the highest detectability can be achieved when utilizing the heterogeneity of these two meters, such as using a few pressure meters with several pipe flow meters to detect the burst events missed by the pressure meter set.

In this study, either a pipe flow meter or pressure meter can be selected for a meter location. Given the predefined *nmeter*, a normalized total meter cost (*TotalMeterCost*) is computed and minimized by the proposed MOMP model. The cost of a pressure meter was assumed to be a unit of 1, whereas that of a pipe flow meter was defined by the multiplier *CostFactor*. For example, $CostFactor = 2$ if the cost of a pipe flow meter is twice that of a pressure meter. Then, $TotalMeterCost = 8$ for five meters comprising two pressure meters and three pipe flow meters with $CostFactor = 2$. Various proportions of the two meters are to be identified in the Pareto optimal solutions of different objective function values (i.e., DP, RF, and CVMR).

Multiobjective Optimal Meter Placement Model

The proposed MOMP model has four objectives: minimize *TotalMeterCost* (F_1), maximize DP (F_2), and minimize RF and CVMR (F_3 and F_4, respectively)

$$\text{Minimize } F_1 = TotalMeterCost \tag{3}$$

$$\text{Maximize } F_2 = \text{DP} \tag{4}$$

$$\text{Minimize } F_3 = \text{RF} \tag{5}$$

$$\text{Minimize } F_4 = \text{CVMR} \tag{6}$$

Although a tradeoff relationship between the first and second objectives has been identified in previous studies, such as in a constrained single-objective model (e.g., Kapelan et al. 2005; Hagos et al. 2016; Simone et al. 2016), relationships between the fourth and other three objectives and between the second and third objectives have not previously been investigated.

Fig. 2 shows a flowchart of the offline process required to provide the input data of the proposed MOMP model as well as the model's structure and submodules. The proposed MOMP model identifies the optimal meter locations for pressure and/or pipe flow meters by using the nondominated sorting genetic algorithm-II (NSGA-II) (Deb et al. 2002) with simulated binary crossover (SBX) (Deb and Agrawal 1994) and polynomial mutation (PM) (Deb and Goyal 1996).

New solutions in the form of a set of integer values indicating meter locations are generated in each generation, and their fitness with respect to the four objectives (i.e., *TotalMeterCost*, DP, RF, and CVMR) is quantified (Fig. 2). DP and RF of a solution are quantified based on the detection and false-alarm matrix, respectively, obtained from the offline process, which applies a statistical process control (SPC) method to control and out-of-control data generated from an EPANET (Rossman 2000) hydraulic model of a network of interest. More details are in the following sections. CVMR is computed with the method described in the "Mechanical

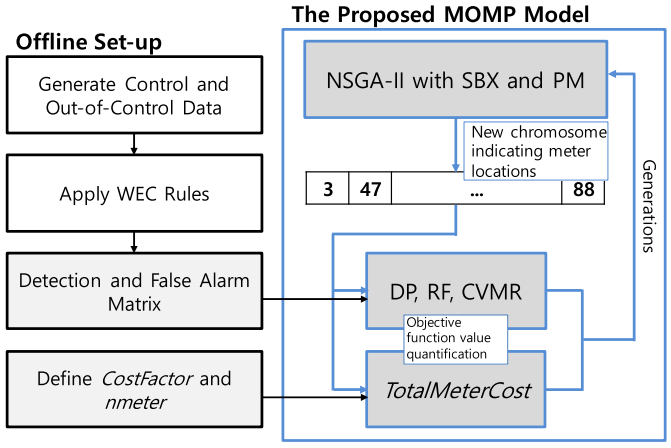

Fig. 2. Schematic diagram of the proposed MOMP model.

J. Water Resour. Plann. Manage., 2018, 144(7): 04018031

Reliability of a Meter Network" section, whereas *TotalMeterCost* is calculated based on the normalized costs of the pressure and pipe flow meters (*CostFactor* is defined before optimization) (Fig. 2). SBX and PM are performed stochastically for a pair of solutions selected from the population. The aforementioned NSGA-II process is repeated until a satisfactory Pareto-optimal meter location set is identified. Each module/component of the proposed MOMP model is described in detail in the following sections.

Western Electric Company Rules

Although various hydroinformatic techniques have been applied for WDS pipe burst detection, such as artificial neural networks (Mounce and Machell 2006), state estimation (Ye and Fenner 2013; Jung et al. 2015), and time-series modeling (Quevedo et al. 2010), the SPC method has become one of the most popular techniques used for WDS pipe burst detection during the last decade (Misiunas et al. 2006; Romano et al. 2010; Palau et al. 2011; Jung et al. 2015). A more detailed review of the aforementioned studies has been provided by Wu and Liu (2017). Some of the most recent studies have put tremendous effort into maximizing the detection effectiveness by developing an advanced hydroinformatic technique that combines pattern matching and binary neural network techniques (Mounce et al. 2014), a multiphase detection method based on a clustering algorithm (Wu et al. 2016), and a practical approach using a renewed concept of the so-called outlier region (Loureiro et al. 2016).

The SPC method applies statistical theory to the process variables (e.g., pipe flow rates and nodal pressures) to identify abnormal patterns that may be caused by bursts (Jung et al. 2015). The basis of the SPC method is the Shewhart control chart, which consists of the mean values (centerline) of the process variables and warming limits (WLs) and control threshold limits (CLs). The latter two are multiples of the standard deviation (σ) on each side of the centerline.

In this study, Western Electric Company (WECO) rules (WECO 1958) were used for a univariate SPC method. These are a set of decision rules for identifying nonrandom patterns in measurements. Several studies have proven the applicability and effectiveness of this method at detecting WDS leakages/pipe bursts (Romano et al. 2010; Jung et al. 2015; Hagos et al. 2016). The WECO rules raise an alarm if the measurements satisfy any of the following four criteria:

- Rule 1: Any single measurement is beyond the $\pm 4\sigma$ CLs.
- Rule 2: Two of three consecutive measurements are beyond $\pm 3\sigma$ WLs.
- Rule 3: Four of five consecutive measurements are beyond $\pm 2\sigma$ WLs.
- Rule 4: Eight consecutive measurements are beyond $\pm 1\sigma$ WLs.

Rules 2–4 should be applied to one side of the centerline at a time. Therefore, a measurement followed by a series of measurements on the other side of the centerline outside the WLs does not trigger an alarm according to Rules 2–4.

Control and Out-of-Control Data Generation

Two sets of pipe flow and pressure data can be generated by using an EPANET hydraulic model of the study network: control and out-of-control data. The former is used to develop the Shewhart control chart for each pipe and node and to calculate RF, whereas the latter is used to compute DP. Control data are generated by considering randomness in nodal demands only, whereas out-of-control data are produced by considering both random demands and pipe bursts.

Several factors of pipe burst events affect pipe burst detection. A big burst is more likely to be detected than a small one. Hagos et al. (2016) found that most bursts are detected at night and in the early morning. A burst event that occurs near a meter retains clear signals of an anomaly. In order to generate pipe burst events of various characteristics, random pipe bursts of different burst magnitudes, initiation times, and locations can be generated and simulated by using an emitter in EPANET. Uniform random sampling is performed to define the three factors of the burst events. The burst flow (*BurstFlow*) is represented as a power function of the nodal pressure

$$BurstFlow = Cp^{\alpha} \tag{7}$$

where C = burst discharge coefficient; p = nodal pressure; and α = power function's exponent. Following the suggestion of Lambert (2001) and Fuchs-Hanusch et al. (2016), α was set to 0.5 based on the assumption of a metal pipe. However, $\alpha = 1.0$ should be used in the absence of knowledge of the pipe materials. Random burst magnitudes are defined by randomly sampling C in a predefined range, and random integer values are chosen for the burst initiation time and location identifier.

Detection and False-Alarm Matrix

As shown in Fig. 2, DP, RF, and CVMR of new solutions generated through selection, SBX, and PM over generations are calculated based on the detection and false-alarm matrices. Their binary elements indicate an alarm for abnormal or natural random events. These are produced by applying the WECO rules to the generated control and out-of-control data. Populating the two matrices is an offline process performed outside the proposed MOMP model. Therefore, the two matrices are the inputs to the proposed model together with *CostFactor* and *nmeter* (Fig. 2).

To populate the detection matrix, the WECO rules are applied to each meter's data one at a time. Fig. 3 shows the multiplication of the example detection matrix **D** and meter configuration matrix **C**, both for pressure meters. The rows of **D** are burst events (total number of events is *ne*), and the columns are potential meter locations (total number of nodes is *nn*). This makes **D** a $ne \times nn$ matrix. For example, the first burst event (Event 1) is detected by the pressure meter located at Node 1, but it is not detected by that at Node 2 (Fig. 3). The false-alarm matrix **F** is constructed in a similar manner but has a value of 1 if a false alarm is issued for a natural random

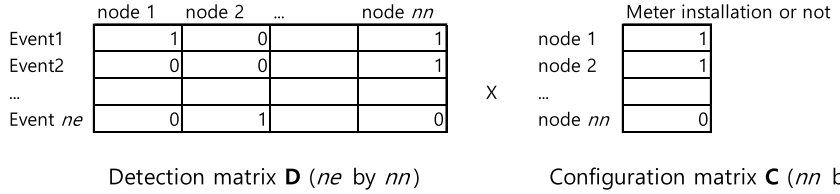

Fig. 3. Multiplication of the detection matrix **D** and configuration matrix **C** to calculate the total DP of the meter network.

event and 0 otherwise. The meter configuration matrix $\mathbf{C}$ ($nn \times 1$ and $np \times 1$ for pressure and pipe flow meters, respectively) is another binary matrix that contains binary values indicating meter installation at a location.

Therefore, DP of a given meter set (*meterset*) is calculated as follows:

$$\mathrm{DP}_{meterset} = \sum_{m \in meterset} \sum_{n=1}^{ne} (\mathrm{D}_{n,m} \times \mathrm{C}_m) \tag{8}$$

in which $D_{n,m}$ [element of $\mathbf{D}$ at (n, m)] = 1 if the mth meter detects the nth burst event, and 0 otherwise; and C_m (mth element of $\mathbf{C}$) = 1 if a meter is installed at the mth location, and 0 otherwise.

Similarly, RF of *meterset* is computed as follows:

$$\mathrm{RF}_{meterset} = \sum_{m \in meterset} \sum_{n=1}^{ne} (\mathrm{F}_{n,m} \times \mathrm{C}_m) \tag{9}$$

in which $F_{n,m}$ [element of $\mathbf{F}$ at (n, m)] = 1 if the mth meter issues an false alarm for the nth natural random event, and 0 otherwise.

NSGA-II with SBX and PM

NSGA-II is a multiobjective version of the genetic algorithm and considers two unique features for the selection process: nondominated ranking and crowding distance. The former feature tries to ensure that a solution superior to others with respect to the considered objectives survives to the next generation, whereas the latter seeks diversity of the Pareto optimal solutions. Deb et al. (2002) offered more details about the two selection methods. The original version of NSGA-II uses general crossover and mutation operators (Deb et al. 2002).

A metaheuristic optimization algorithm with well-balanced intensification and diversification yields high-quality optimal solutions (Kim 2016). That is, the algorithm should have both the capacity to search a broad area of solution space but also the ability to seek promising regions. In this study, SBX and PM were used to improve the search performance of NSGA-II. They stochastically control the deviation of children solutions from parent solutions by crossover and mutation distribution indices (CDI and MDI, respectively) which are the shape parameters for a polynomial probability distribution.

Given the CDI value, the SBX operator generates two children solutions x_c^1 and x_c^2 from the two parent solutions x_p^1 and x_p^2 as follows:

$$x_c^1 = 0.5[(1+\beta)x_p^1 + (1-\beta)x_p^2] \tag{10}$$

$$x_c^2 = 0.5[(1-\beta)x_p^1 + (1+\beta)x_p^2] \tag{11}$$

where

$$\beta = \begin{cases} (2u)^{1/(\mathrm{CDI}+1)} & \text{if } u \le 0.5 \\ \left(\dfrac{1}{2(1-u)}\right)^{1/(\mathrm{CDI}+1)} & \text{otherwise} \end{cases}$$

where u = randomly sampled real number; and $u \in (0, 1)$. Fig. 4 shows the probability distributions of $[\varepsilon(\beta)]$ for two different CDI values: CDI = 2.0 and 20. Although the shape of a distribution is commonly symmetric around a single sharp peak at $\beta = 1$ (parent solution's location), the slopes of the rising and falling limbs and the peak/highest value are different. Therefore, the probability of producing children solutions distant from the parent solutions is higher with CDI = 2.0 than with CDI = 20. More details on SBX and PM (e.g., PM formulations) have been given by Jung et al. (2017).

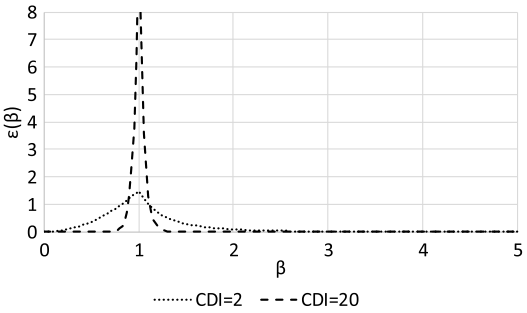

Fig. 4. Probability distributions of the simulated binary crossover with two crossover distribution index values.

Study Network

The proposed MOMP model was applied to the modified Austin network (Jung and Lansey 2015; Hagos et al. 2016; Jung et al. 2016) and Balerma network (Reca and Martínez 2006). As shown in Fig. 5(a), the Austin network is an urban drinking-water distribution network and consists of 126 nodes and 90 pipes ($nn = 126$ and $np = 90$) supplied by a single reservoir and one pumping station, where four identical pumping units maintain a constant total head of water. The total system demand of the network is 726 L/s. A transmission line of 762-, 1,219-, and 1,524-mm diameter pipes (30-, 48-, and 60-in., respectively) is laid through the middle of the network to deliver subarea demands from the single source. The Austin network is loop-dominated with few local branched sections (e.g., at the northeast and south ends). The biggest pipe is the 1,829-mm diameter (72-in.) source pipe, whereas the smallest pipe size is 152 mm (6 in.).

Fig. 5(b) shows the Balerma network, which is an irrigation network supplied by four reservoirs and composed of 443 nodes and 454 pipes ($nn = 443$ and $np = 454$) (Reca and Martínez 2006). The total system demand is 1,790 L/s, which is approximately 2.5 times that of the Austin network. A least-cost design was used for the Balerma network. Main pipelines over 200-mm in diameter and stemming from each reservoir are connected throughout the network to make a looped network. However, the network configuration can be visualized as a branched system because of the many pendant lines, each with two to four pipes, tapped into the main pipes [Fig. 5(b)]. Pipe sizes range from 113 to 582 mm for the Balerma network. Although approximately 95% of the pipes are smaller than 400 mm in diameter, 17.8% pipes are greater than 600 mm. The average pipe size is 424 mm in the Austin network and 208 mm in the Balerma network.

Three time-series data sets were generated for the offline analysis to populate the detection and false-alarm matrices (Fig. 2). First, a normal 2,000-day time series of the nodal pressures and pipe flow rates at a 5-min time step was generated by using the networks' hydraulic model to construct the Shewhart control chart of each variable. Gaussian random time series of the nodal demands were generated by assuming no spatial correlation but a strong temporal correlation because of the underlying diurnal pattern and then input to the model. Each nodal demand was assumed to have a CV of 0.1.

A control data set and out-of-control data set were used to construct the false-alarm and detection matrices, respectively. In total, 1,000 burst events and 1,000 natural random events were generated.

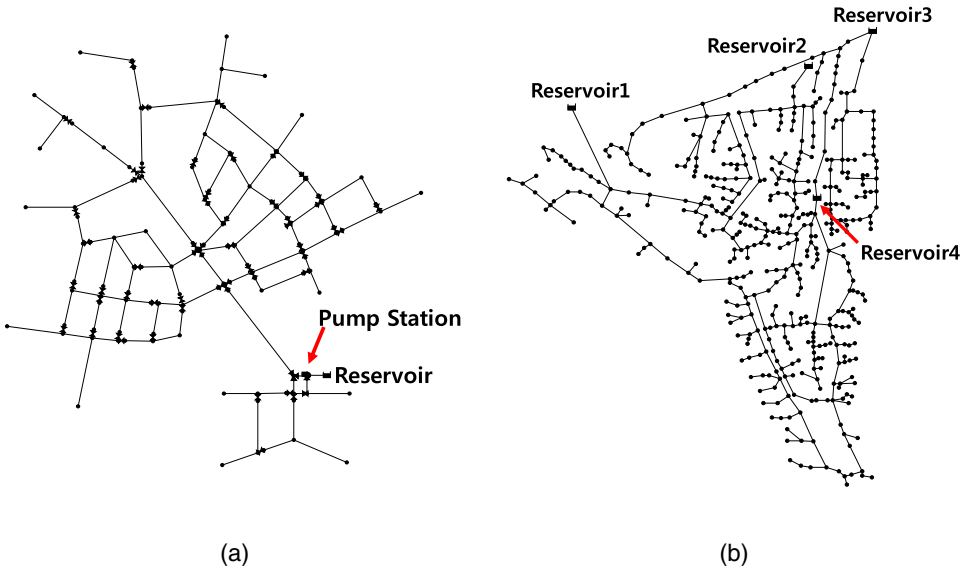

Fig. 5. Layouts of the two study networks: (a) Austin; and (b) Balerma.

The burst discharge coefficient Cs was sampled over the range of 1–100 in both networks.

NSGA-II with SBX and PM started its search with randomly generated solutions, i.e., a string of random integer values sampled over the range of 1 to $nn + np$, which indicated the locations of the nodal pressure and pipe flow meters. Only a single meter could be installed per node/pipe. Several parameters of NSGA-II with SBX and PM were determined from a sensitivity analysis to find a final Pareto solution of high quality; this is not presented in this paper. A CDI of 20 and MDI of 20 were used for SBX and PM, respectively, of NSGA-II. Therefore, children solutions close to parent solutions were produced more frequently than parent-resembling solutions [e.g., when CDI and MDI were both 2.0 (Fig. 4)]. The final Pareto solutions were determined by running NSGA-II with SBX and PM for a population of 200 evolving over 20,000 generations. The crossover and mutation rates were 0.9 and 0.1, respectively.

Application Results

Pareto-Optimal Meter Sets Obtained Considering Three Objectives (CostFactor = 1)

First, the proposed MOMP model was applied to the two study networks under the assumption that $CostFactor = 1$ (i.e., the two types of meters cost the same). Therefore, the model's objectives [i.e., four objectives given in Eqs. (3)–(6)] were relaxed to maximize DP [Eq. (4)], minimize RF [Eq. (5)], and minimize CVMR [Eq. (6)]. Based on preliminary sensitivity analyses for finding an adequate number of meters, it was assumed that a total of seven meters was available for both networks. Fig. 6 shows the projections of the final Pareto solutions for the Austin network onto three-dimensional [Fig. 6(a)] and two-dimensional plots [Figs. 6(b–d)]. Fig. 6(a) represents the ratio of pipe flow meters as a gray color for the Austin network. Fig. 7 shows the same results but for the Balerma network.

Each axis is scaled so that the utopian point of (DP, RF, CVMR) equal to (1, 0, 0) is located at the frontmost corner of the three-dimensional plots in Figs. 6(a) and 7(a). Although the relative position of the Pareto solutions is not easy to visually identify in Figs. 6(a) and 7(a), the two-dimensional plots of each pair of the three objectives [e.g., Fig. 6(b) for DP and RF, Fig. 6(c) for DP and CVMR, and Fig. 6(d) for RF and CVMR] provide easier interpretation. The plot axes are in the same range for relative comparison between the two study networks (Figs. 6 and 7). Nondominated solutions with respect to two objectives were also identified in post-optimization analysis and marked as asterisk points in the two-dimensional plots [Figs. 6(b–d) and 7(b–d)]. These were referred to when interpreting the relation between each pair of the three objectives.

Regardless of network, a nonlinear relationship was confirmed between DP and RF. DP can be increased by allowing more false alarms [Figs. 6(b) and 7(b)]. For the Austin network, the water utility manager would want to select the optimal meter location set with DP = 0.975, RF = 0.08, and CVMR = 0.02 (the asterisk solution indicated by an arrow in Fig. 6(b) is a practical solution among the mathematical Pareto-optimal solutions) because there are marginal DP increases with significant RF increases beyond the solution [left side of Fig. 6(b)]. It was easier to detect pipe bursts in the Balerma network than in the Austin network; the overall DP was higher and RF was lower for the Balerma network with the looped configuration [Fig. 5(b)] because anomalous events that occur at a location can affect hydraulics at other sites of the network (Jung et al. 2015). This resulted in the final solution being positioned at the lower left corner of Fig. 7(b) for the Balerma network.

Fig. 8 shows the scatter plot of the pipe flow meter ratio and the three objectives considered in this study for the Austin network. DP tended to increase as more pipe flow meters were included in the seven meters [Figs. 6(a) and 8(a)]. Especially, the filled shade of the solution points indicating the pipe flow meter ratio changed along the DP axis, as shown in Fig. 6(a). This is because pressure meters detect common bursts, whereas pipe flow meters detect different unique bursts (Hagos et al. 2016). That is, a common burst will be detected by most pressure meters, whereas a unique burst will only be detected by a certain pipe flow meter(s). Higher detectability (i.e., higher DP and lower RF) can be obtained with the former than the latter (Jung et al. 2015). Therefore, the best strategy for meter location is to combine a few pressure meters and multiple pipe flow meters so that the latter complements the former. Including more pipe flow meters increased RF [Fig. 8(b)].

A similar relationship between the pipe flow ratio and three objectives was also obtained for the Balerma network but is not

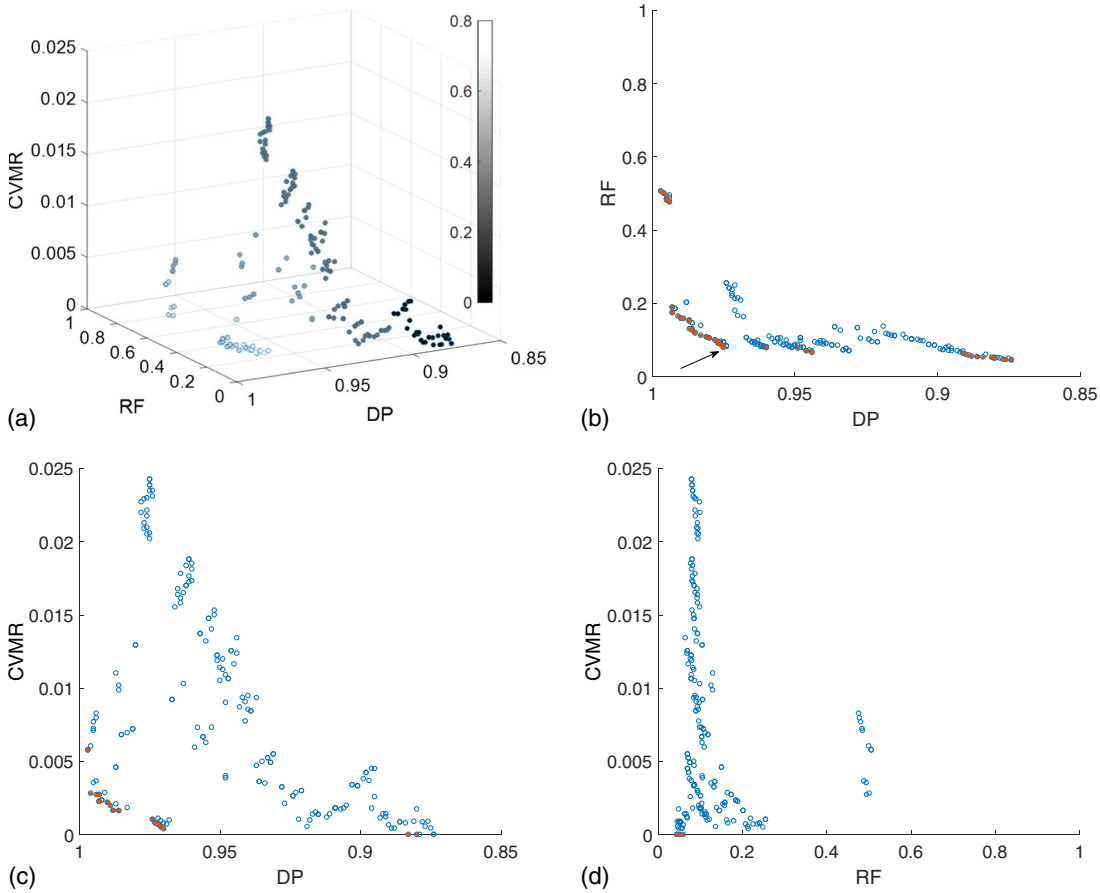

Fig. 6. Pareto-optimal solutions obtained from the proposed MOMP model with three objectives (maximize DP, minimize RF, and minimize CV_{MR}) for the Austin network given that seven meters are available: (a) three-dimensional plots of DP and RF; (b) two-dimensional plots of DP and RF; (c) DP and CVMR; and (d) RF and CVMP. The solution points in (a) are filled with a grayscale representing each solution's pipe flow meter ratio. The asterisks in (b–d) are nondominated solutions with respect to the two objectives considered in each two-dimensional plot.

presented here. Although the final Pareto solutions for the Balerma network were only divided into those without pipe flow meters and those with a single pipe flow meter (pipe flow meter ratio of 0.143) [Fig. 7(a)], up to five of the seven available meters (ratio of 0.714) were pipe flow meters for the Austin network [Figs. 6(a) and 8].

A tradeoff relationship was confirmed between DP and the meter network's mechanical reliability [Figs. 6(c) and 7(c)], whereas no significant relation was found between RF and the latter [Figs. 6(d) and 7(d)]. For both networks, CVMR increased with DP. The asterisk nondominated solutions for the Balerma network had very high DP (i.e., 0.971–1.0) and CVMR ranging from 0 to 0.01, which resulted in the almost vertical frontal curve shown in Fig. 7(c). The relationship seems to originate from the increased DP for optimal meter sets with a high ratio of pipe flow meters. As more pipe flow meters were included in a meter set, the variation in the partially impaired meter network's DPs increased [i.e., increased $\sigma(\mathrm{DP}_{f,i})$ in Eq. (2)], retaining the average DP [i.e., retaining $\mathrm{avg}(\mathrm{DP}_{f,i})$ in Eq. (2)]. This finally resulted in a high CVMR.

In contrast, a very high CVMR could be obtained with only pressure meters. Some asterisk nondominated solutions had CVMR of 0, as shown in Figs. 6(c and d) and 7(c and d). For example, an optimal meter set with DP of 0.88 and RF of 0.052 for the Austin network had CVMR of 0, which is the highest mechanical reliability level. The meter set only consisted of seven pressure meters; each meter's failure identically resulted in a total DP for the meter network of 0.88 [i.e., the variance $\sigma(\mathrm{DP}_{f,i}) = 0$ with double precision]. Individual meters had similar DPs of either 0.868, 0.87, or 0.871. Therefore, only pressure meters should be included in a meter network to assure high mechanical reliability.

Pareto-Optimal Meter Sets Obtained Considering Full Four Objectives (CostFactor = 2)

Finally, the Pareto-optimal meter sets were identified when all four objectives [Eqs. (3)–(6)] were considered and $CostFactor = 2$. These were projected in three-dimensional [e.g., Fig. 9(a) for the Austin network] and two-dimensional plots [e.g., Fig. 9(b)], similar to Figs. 6 and 7. Although the solution points are positioned based on the three objective values of DP, RF, and CVMR in three-dimensional space, *TotalMeterCost* is represented by the grayscale filling the points, where lighter solutions are more expensive than darker ones, as shown in Fig. 9(a).

TotalMeterCost of the Pareto solutions ranged from 7 to 12 for the Austin network and from 8 to 9 for the Balerma network. This indicated that maximums of five and two pipe flow meters (pipe flow ratios of 0.714 and 0.143, respectively) were included in the Austin and Balerma networks, respectively. The maximum number of pipe flow meters included for each network was the same as that of the solutions obtained from the three-objective optimization [Figs. 6(a) and 7(a)].

Regardless of the network, the Pareto-optimal fitness landscape constructed based on the three objective values from the

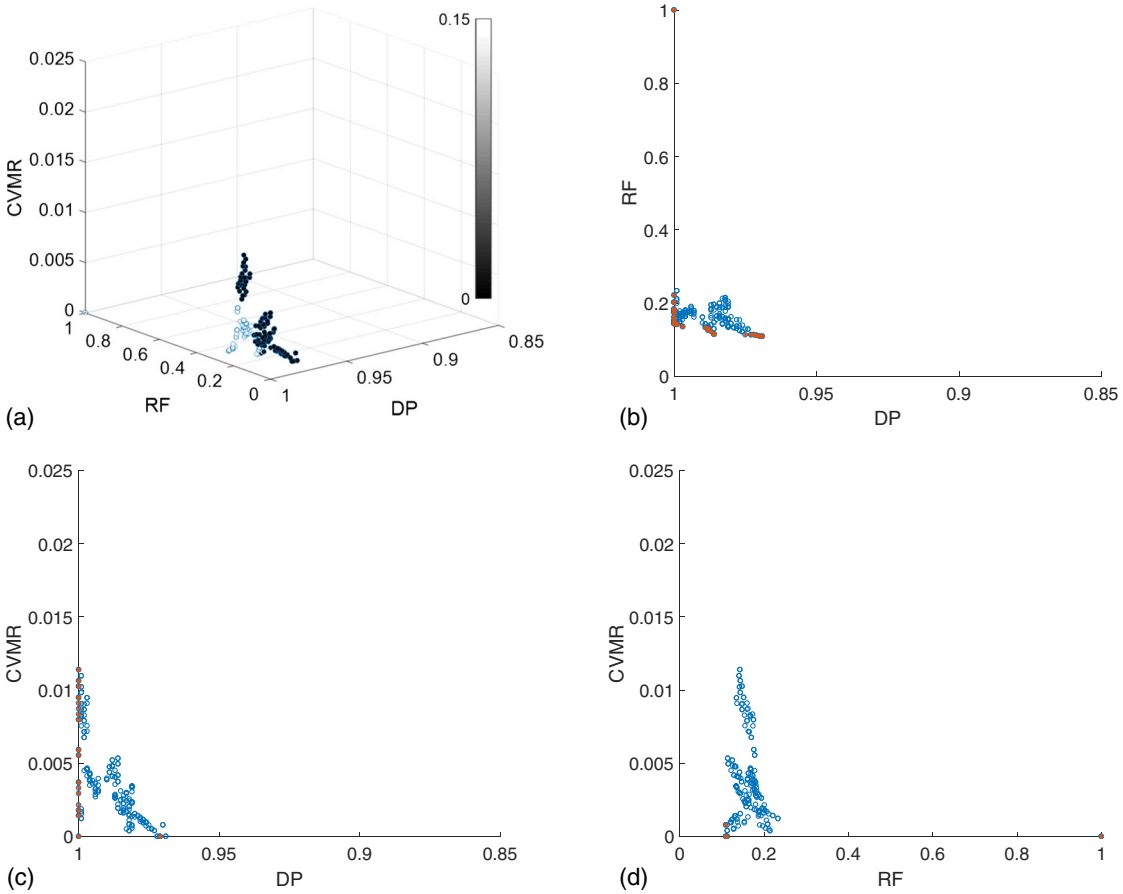

Fig. 7. Pareto-optimal solutions obtained from the proposed MOMP model with three objectives (maximize DP, minimize RF, and minimize CV_{MR}) for the Balerma network given that seven meters are available: (a) three-dimensional plots of DP and RF; (b) two-dimensional plots of DP and RF; (c) DP and CVMR; and (d) RF and CVMP. The solution points in (a) are filled with a grayscale representing each solution's pipe flow meter ratio. The asterisks in (b–d) are nondominated solutions with respect to the two objectives considered in each two-dimensional plot.

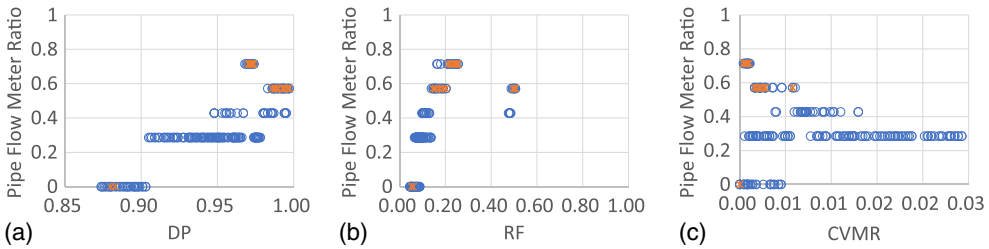

Fig. 8. Scatter plots of the pipe flow meter ratio and three objective functions for the Austin network: (a) DP; (b) RF; and (c) CVMR. Asterisks are nondominated solutions with respect to the two objectives considered in each two-dimensional plot.

four-objective optimization was similar to that drawn by the three-objective optimization results [e.g., Figs. 6(a) and 9(a)]. For the Austin network, *TotalMeterCost* increased along the axis of DP [Fig. 9(a)], which indicates that the meter cost and pipe flow meter ratio increased with DP. The pattern of the grayscale color change in Fig. 9(a) is similar to that in Fig. 6(a), even though *TotalMeterCost* was not optimized in the three-objective optimization. The Pareto fronts from the two optimizations presented in the two-dimensional plots were also quite similar [Fig. 9(b)].

These results were presented because it was very challenging to find solutions that dominated all four objectives. Thus, the three-objective solutions were revisited in the four-objective optimization, even though they were not provided as initial solutions. The optimization results of $CostFactor = 1$ and 3 (not presented here) had similar patterns to those of $CostFactor = 2$ with respect to the maximum number of pipe flow meters included, shape of the Pareto optimal fitness landscape, and revisited three-objective optimization solutions ($CostFactor = 1$).

Pareto-Optimal Meter Layout Comparison

In order to check the meter locations determined from the MOMP model, a representative solution was selected based on engineering judgement from each study network. Each had the same $TotalMeterCost = 9$ (two pipe flow meters were included) and similar RF of approximately 0.11. In Fig. 10, the selected solution

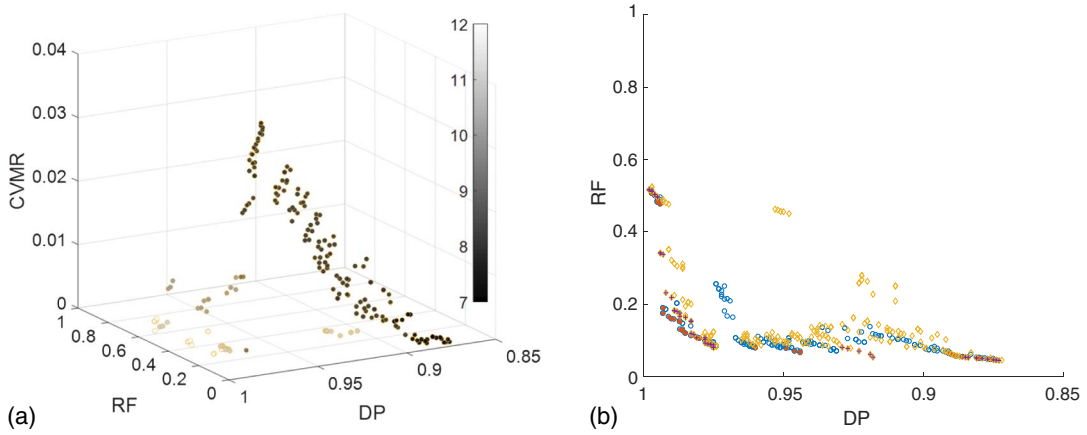

Fig. 9. Pareto-optimal solutions obtained with full four objectives (minimize *TotalMeterCost*, maximize DP, minimize RF, and minimize CVMR) for the Austin network given that seven meters are available and *CostFactor* = 2 (pipe flow meter cost is twice the pressure meter cost): (a) three-dimensional plot with *TotalMeterCost* value on a filled color scale; and (b) two-dimensional plots of DP and RF compared with Pareto-optimal solutions when $CostFactor = 1$ [Figs. 6(c and d)]. In (b), the Pareto-optimal solutions obtained with $CostFactor = 2$ are diamonds, nondominated solutions with respect to DP and RF are crosses, and solutions with $CostFactor = 1$ brought from Fig. 6(b) maintain their symbol styles.

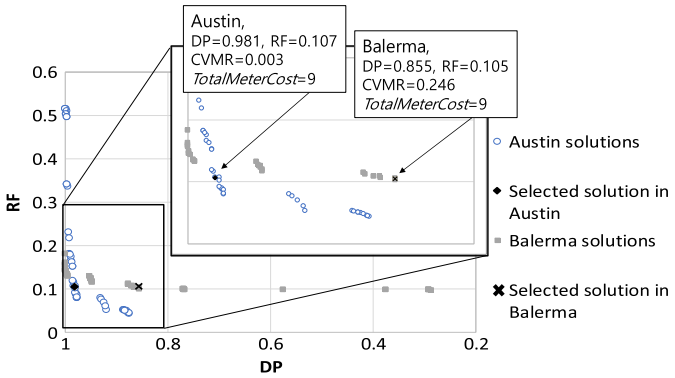

Fig. 10. Projection of the Pareto-optimal solutions for the two study networks obtained assuming $CostFactor = 2$ onto the two-dimensional plot of DP and RF. A similar RF and same *TotalMeterCost* solution (RF ~ 0.1 and $TotalMeterCost = 9$) were selected from each network. These are indicated by an arrow from an information box containing the values of the four objectives.

for the Austin network of DP = 0.981 and CVMR = 0.003 is marked as a diamond among all Pareto front solutions, which are represented as open circles in the two-dimensional plot of DP and RF. The solution of DP = 0.855 and CVMR = 0.246 was selected for the Balerma network and marked as a cross. Among the solutions with an acceptable RF (i.e., <10%), those of the Austin network had a higher detection effectiveness than those of the Balerma network (Fig. 10), as confirmed in the previous section. The Balerma network's solutions dominated the Austin network's solutions when DP > 0.99 (Fig. 10), although these solutions would not be preferred because of the high RF > 0.15.

Fig. 11 shows the meter locations of the selected solutions. It was confirmed that a common strategy was applied for pipe flow meters, whereas different network-specific approaches were adopted for the pressure meters. Regardless of the network, pipe flow meters were placed at informative locations where either a large volume of water demand flowed or there were interconnections between subareas. That is, Meters 1 and 2 (pipe flow meters) were installed downstream of the single source in the Austin network [Figs. 5(a) and 11(a)]. For the Balerma network, Meter 62 was placed at the interconnection pipe between subareas supplied by transmission lines with pipe sizes of 452 and 362 mm, and Meter 416 was located downstream of the north-end source supplying the second-largest volume of water demand among the four sources [Figs. 5(b) and 11(b)].

Although the source supplying the largest volume of flow was positioned in the middle of the loops [i.e., reservoir on the left side of the pressure sets in the inset of Fig. 11(b)], the north-end reservoir's peripheral hydraulics helped achieve high detectability in addition to supplying water demand (e.g., detecting pipe bursts missed by pipe flow meters). That is, all pressure meters were installed one after the other (Meters 191, 193, 200, 203, and 204) in the downstream subsection where the nodal elevation was highest within the network [Fig. 11(b)]. Therefore, pressure drops from pipe bursts at the low-pressure nodes were more apparent compared to their normal average pressure than those at other nodes. On the other hand, pressure meters were located either near the end of network (Meters 11 and 65) or in the middle of a looped subsection (Meter 112) for the Austin network [Fig. 11(a)].

As indicated in Table 1, the main detector was a pipe flow meter for the Balerma network (i.e., Pipe flow meter 62 had the highest DP of 0.673), whereas it was a pressure meter for the Austin network (i.e., DP of the pressure meters was higher than 0.86). These results highlight that the role of each type of meter varies for different networks of different configurations, characteristics, and numbers of components.

Different distributions of detection roles were also found with the detection matrix. Fig. 12 shows part of the detection matrix for the selected Pareto-optimal meter sets of the two study networks. Burst events are in rows, meters are in columns, and a solid cell indicates an event detected by a meter. The pressure meters were confirmed to detect common bursts, with the pressure meters identifying different bursts. These results agree with those of Hagos et al. (2016). A new and noteworthy finding is that using the proposed MOMP model could ensure that the two types of meters did not overlap in the optimal meter networks for maximizing DP and optimizing other objectives. For example, the two pipe flow meters in the Austin network seemed to be designed to detect bursts missed by pressure meters, and the pressure meters in the Balerma network were intended to detect the remaining pipe bursts missed by the two pipe flow meters (Fig. 12).

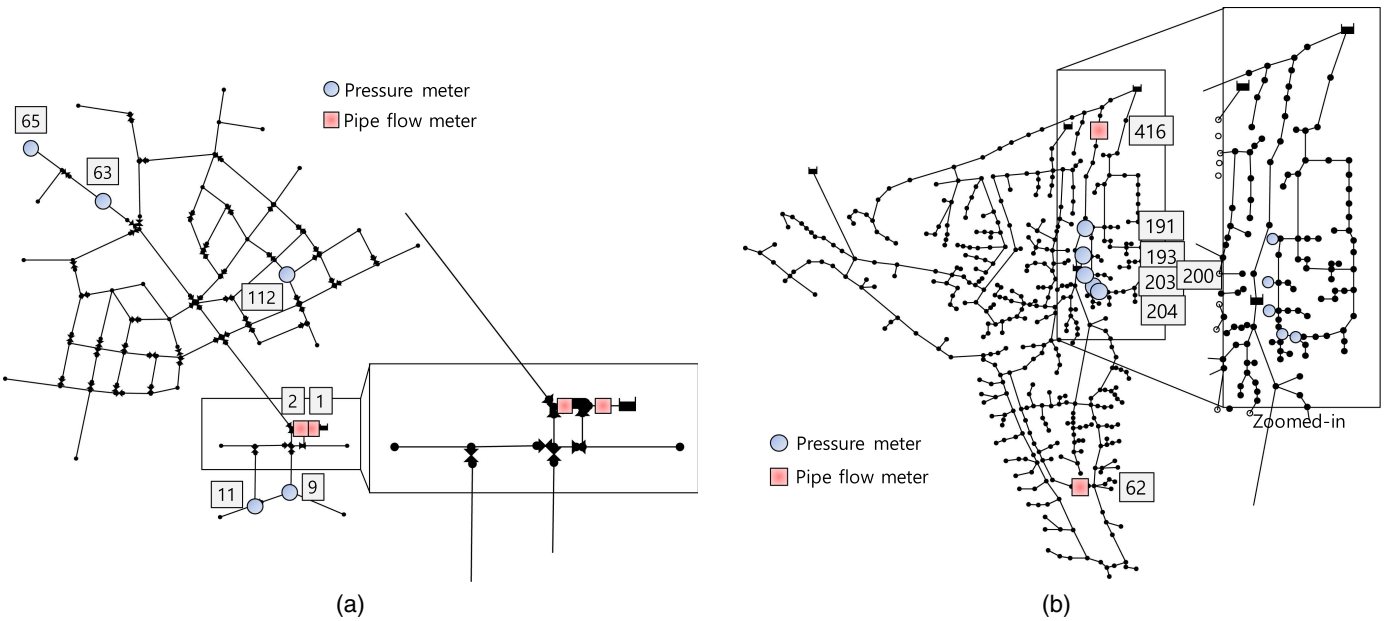

Fig. 11. Meter layout of the selected Pareto solutions in Fig. 10 for (a) Austin; and (b) Balerma networks.

Table 1. Individual meters' DP with the optimal meter sets selected in Fig. 10 for the two study networks

Network	Meter location	Location number	DP
Austin	Pipe	1	0.847
		2	0.827
	Node	9	0.868
		11	0.863
		63	0.869
		65	0.872
		112	0.865
Balerma	Pipe	62	0.673
		416	0.180
	Node	203	0.197
		204	0.197
		193	0.197
		191	0.205
		200	0.196

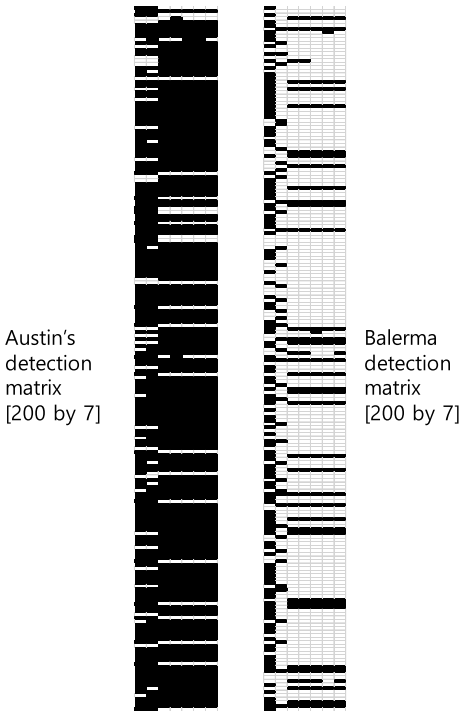

Fig. 12. Detection matrix of the selected Pareto solution in Fig. 10 for the first 200 burst events in the two study networks. Rows are 200 burst events, and columns are seven meters. The first two columns are pipe flow meters. The order of the meters from left to right is equivalent to the order in Table 1 from top to bottom. A solid cell (i, j) indicates that the event i was detected by meter j.

Summary and Conclusions

This paper presented a MOMP model for WDS pipe burst detection to minimize the normalized total meter cost (i.e., *TotalMeterCost*), maximize DP, minimize RF, and maximize the meter network's mechanical reliability. A novel method based on single-meter failure simulation was used to quantify the CV of DPs of a partially impaired meter network (i.e., CVMR); this was used as an indicator of the mechanical reliability. The optimal ratio between pressure and pipe flow meters was identified given a predefined number of meters (i.e., *nmeter*) in the proposed model, where the normalized meter cost of the latter is defined as *CostFactor* assuming that the former's cost is equal to 1. The proposed MOMP model was demonstrated on the Austin and Balerma networks with different configurations, characteristics, and numbers of components under the assumption that a total of seven meters was available.

First, the proposed model was applied to the two study networks assuming $CostFactor = 1$, so $TotalMeterCost = 7$ for all solutions. The results confirmed that, regardless of the network, DP increased when more false alarms were allowed (i.e., by increasing RF), and there was a marginal DP increase but significant RF increase for high-DP solutions. The Balerma network had a higher

overall detectability than the Austin network because of the former's high connectivity. Although no significant relation between RF and CVMR was observed, a nonlinear tradeoff relationship was found between DP and CVMR (i.e., CVMR increased with DP) for both networks. High-DP solutions incorporated more pipe flow meters, which have relatively low DP but detect different unique burst events, whereas pressure meters detect common burst events. This caused a high variation in the partially impaired meter network's DPs, which resulted in a high CVMR. Very high CVMP could be achieved by including pressure meters only, which suggests that pressure meters should be used to ensure high mechanical reliability.

Then, the multiobjective problems were solved when $CostFactor = 2$ (i.e., the pipe flow meter cost was twice the pressure meter cost). The Austin and Balerma networks included maximums of five and two pipe flow meters, respectively. These are the same maximum values for the solution obtained from the meter placement with $CostFactor = 1$. The Pareto-optimal fitness landscape when $CostFactor = 2$ was similar to that of $CostFactor = 1$ because the solutions obtained from the latter optimization had a nondominated nature with respect to most of the four objectives.

Finally, an optimal meter layout derived from the proposed MOMP model was selected for each network to have the same $TotalMeterCost = 9$ and RF of around 0.11 and compared with respect to the adopted meter location strategies. The selected solution for the Austin network had a higher DP and lower CVMR than that for the Balerma network.

The adopted meter location rules were as follows: pipe flow meters were located at informative locations where either a large volume of water demand flowed or interconnections between subareas, whereas different network-specific approaches were used for pressure meters. For the Balerma network, all pressure meters were installed downstream of a low-pressure zone. On the other hand, pressure meters were located either near the end of network or in the center of a looped subsection for the Austin network. The main detector was a pipe flow meter for the Balerma network but a pressure meter for the Austin network. This indicates that the role of each type of meter varies for different networks of different characteristics. Therefore, the proposed MOMP can be a useful tool for determining the optimal meter location and best combination of meters for high detectability and mechanical reliability of a specific network of interest.

This study had several limitations that future research must address. First, this study presented the MOMP results assuming that seven meters were available in total, as determined from preliminary sensitivity analyses. A thorough sensitivity analysis should be performed for a network to determine how the relationships among the four objectives (*TotalMeterCost*, DP, RF, and CVMR) change with different numbers of meters. Second, the correlation between CVMRs under single- and multiple-failure conditions should be investigated to confirm the representativeness of the single-failure approach. In addition, meter failure probability can be considered when quantifying CVMR based on a Monte Carlo simulation. Third, the performance of NSGA-II with SBX and PM in the multiobjective solution space should be investigated in order to better find optimal meter sets of high quality. Finally, the proposed meter network mechanical reliability can be considered in OMP problems for other purposes (e.g., WDS state estimation).

Acknowledgments

This work was supported by a grant from the National Research Foundation (NRF) of Korea funded by the Korean government (MSIP) (No. 2016R1A2A1A05005306).

References

Abbott, M. B. 1999. "Introducing hydroinformatics." *J. Hydroinf.* 1 (1): 3–19.

Bragalli, C., M. Fortini, and E. Todini. 2016. "Enhancing knowledge in water distribution networks via data assimilation." *Water Resour. Manage.* 30 (11): 3689–3706. https://doi.org/10.1007/s11269-016-1372-0.

Brion, L. M., and L. W. Mays. 1991. "Methodology for optimal operation of pumping stations in water distribution systems." *J. Hydraul. Eng.* 117 (11): 1551–1569.

Deb, K., and R. B. Agrawal. 1994. "Simulated binary crossover for continuous search space." *Technical Rep. IITK/ME/SMD-94027*. Kanpur, Uttar Pradesh, India: Indian Institute of Technology.

Deb, K., and M. Goyal. 1996. "A combined genetic adaptive search (GeneAS) for engineering design." *Comput. Sci. Inf.* 26 (4): 30–45.

Deb, K., A. Pratap, S. Agarwal, and T. A. M. T. Meyarivan. 2002. "A fast and elitist multiobjective genetic algorithm: NSGA-II." *IEEE Trans. Evol. Comput.* 6 (2): 182–197. https://doi.org/10.1109/4235.996017.

Farley, B., S. R. Mounce, and J. B. Boxall. 2010. "Field testing of an optimal sensor placement methodology for event detection in an urban water distribution network." *Urban Water J.* 7 (6): 345–356. https://doi.org/10.1080/1573062X.2010.526230.

Fuchs-Hanusch, D., D. Steffelbauer, M. Günther, and D. Muschalla. 2016. "Systematic material and crack type specific pipe burst outflow simulations by means of EPANET2." *Urban Water J.* 13 (2): 108–118. https://doi.org/10.1080/1573062X.2014.994006.

Hagos, M., D. Jung, and K. E. Lansey. 2016. "Optimal meter placement for pipe burst detection in water distribution systems." *J. Hydroinf.* 18 (4): 741–756. https://doi.org/10.2166/hydro.2016.170.

Huang, H., T. Tao, and K. Xin. 2012. "Optimal pressure meters placement for bursts detection based on SOM." In *Proc., 14th Water Distribution Systems Analysis Conf.*, 1127–1137. Barton, Australia: Engineers Australia.

Jung, D., Y. H. Choi, and J. H. Kim. 2016. "Optimal node grouping for water distribution system demand estimation." *Water* 8 (4): 160. https://doi.org/10.3390/w8040160.

Jung, D., Y. H. Choi, and J. H. Kim. 2017. "Multiobjective automatic parameter calibration of a hydrological model." *Water* 9 (3): 187. https://doi.org/10.3390/w9030187.

Jung, D., D. Kang, J. Liu, and K. Lansey. 2015. "Improving the rapidity of responses to pipe burst in water distribution systems: A comparison of statistical process control methods." *J. Hydroinf.* 17 (2): 307–328. https://doi.org/10.2166/hydro.2014.101.

Jung, D., and J. H. Kim. 2017. "State estimation network design for water distribution systems." *J. Water Resour. Plann. Manage.* 144 (1): 06017006. https://doi.org/10.1061/(ASCE)WR.1943-5452.0000862.

Jung, D., and K. Lansey. 2015. "Water distribution system burst detection using a nonlinear Kalman filter." *J. Water Resour. Plann. Manage.* 141 (5): 04014070. https://doi.org/10.1061/(ASCE)WR.1943-5452.0000464.

Kang, D., and K. Lansey. 2010. "Optimal meter placement for water distribution system state estimation." *J. Water Resour. Plann. Manage.* 136 (3): 337–347. https://doi.org/10.1061/(ASCE)WR.1943-5452.0000037.

Kapelan, Z. S., D. A. Savic, and G. A. Walters. 2003. "Multiobjective sampling design for water distribution model calibration." *J. Water Resour. Plann. Manage.* 129 (6): 466–479. https://doi.org/10.1061/(ASCE)0733-9496(2003)129:6(466).

Kapelan, Z. S., D. A. Savic, and G. A. Walters. 2005. "Optimal sampling design methodologies for water distribution model calibration." *J. Hydraul. Eng.* 131 (3): 190–200. https://doi.org/10.1061/(ASCE)0733-9429(2005)131:3(190).

Kim, J. H. 2016. "Harmony search algorithm: A unique music-inspired algorithm." *Procedia Eng.* 154: 1401–1405. https://doi.org/10.1016/j.proeng.2016.07.510.

Lambert, A. 2001. "What do we know about pressure-leakage relationships in distribution systems?" In *Proc., IWA Conf. on Systems Approach to Leakage Control and Water Distribution System Management*, 89–96. London: International Water Association.

Loureiro, D., C. Amado, A. Martins, D. Vitorino, A. Mamade, and S. T. Coelho. 2016. "Water distribution systems flow monitoring and anomalous event detection: A practical approach." *Urban Water J.* 13 (3): 242–252. https://doi.org/10.1080/1573062X.2014.988733.

Misiunas, D., J. Vítkovský, G. Olsson, M. Lambert, and A. Simpson. 2006. "Failure monitoring in water distribution networks." *Water Sci. Technol.* 53 (4–5): 503–511. https://doi.org/10.2166/wst.2006.154.

Mounce, S. R., and J. Machell. 2006. "Burst detection using hydraulic data from water distribution systems with artificial neural networks." *Urban Water J.* 3 (1): 21–31. https://doi.org/10.1080/15730620600578538.

Mounce, S. R., R. B. Mounce, T. Jackson, J. Austin, and J. B. Boxall. 2014. "Pattern matching and associative artificial neural networks for water distribution system time series data analysis." *J. Hydroinf.* 16 (3): 617–632. https://doi.org/10.2166/hydro.2013.057.

Palau, C. V., F. J. Arregui, and M. Carlos. 2011. "Burst detection in water networks using principal component analysis." *J. Water Resour. Plann. Manage.* 138 (1): 47–54. https://doi.org/10.1061/(ASCE)WR.1943-5452.0000147.

Pérez, R., V. Puig, J. Pascual, A. Peralta, E. Landeros, and L. Jordanas. 2009. "Pressure sensor distribution for leak detection in Barcelona water distribution network." *Water Sci. Technol. Water Supply* 9 (6): 715–721. https://doi.org/10.2166/ws.2009.372.

Quevedo, J., V. Puig, G. Cembrano, J. Blanch, J. Aguilar, D. Saporta, G. Benito, M. Hedo, and A. Molina. 2010. "Validation and reconstruction of flow meter data in the Barcelona water distribution network." *Control Eng. Pract.* 18 (6): 640–651. https://doi.org/10.1016/j.conengprac.2010.03.003.

Reca, J., and J. Martínez. 2006. "Genetic algorithms for the design of looped irrigation water distribution networks." *Water Resour. Res.* 42 (5): W05416. https://doi.org/10.1029/2005WR004383.

Reca, J., and J. Martínez. 2006. "Genetic algorithms for the design of looped irrigation water distribution networks." *Water Resour. Res.* 42 (5): W05416. https://doi.org/10.1029/2005WR004383.

Romano, M., Z. Kapelan, and D. A. Savić. 2010. "Real-time leak detection in water distribution systems." In *Proc., 12th Annual Conf. on Water Distribution Systems Analysis*, 1074–1082. Reston, VA: ASCE.

Rossman, L. 2000. *EPANet2 user's manual*. Washington, DC: US Environmental Protection Agency.

Sankary, N., and A. Ostfeld. 2017. "Scaled multiobjective optimization of an intensive early warning system for water distribution system security." *J. Hydraul. Eng.* 143 (9): 04017025. https://doi.org/10.1061/(ASCE)HY.1943-7900.0001317.

Sela Perelman, L., W. Abbas, X. Koutsoukos, and S. Amin. 2016. "Sensor placement for fault location identification in water networks." *Automatica* 72 (C): 166–176. https://doi.org/10.1016/j.automatica.2016.06.005.

Simone, A., O. Giustolisi, and D. B. Laucelli. 2016. "A proposal of optimal sampling design using a modularity strategy." *Water Resour. Res.* 52 (8): 6171–6185. https://doi.org/10.1002/2016WR018944.

Steffelbauer, D. B., and D. Fuchs-Hanusch. 2016. "Efficient sensor placement for leak localization considering uncertainties." *Water Resour. Manage.* 30 (14): 5517–5533. https://doi.org/10.1007/s11269-016-1504-6.

Taormina, R., and S. Galelli. 2017. "Real-time detection of cyber-physical attacks on water distribution systems using deep learning." In *Proc., World Environmental and Water Resources Congress 2017*, 469–479. Reston, VA: ASCE.

Taormina, R., S. Galelli, N. O. Tippenhauer, E. Salomons, and A. Ostfeld. 2017. "Characterizing cyber-physical attacks on water distribution systems." *J. Water Resour. Plann. Manage.* 143 (5): 04017009. https://doi.org/10.1061/(ASCE)WR.1943-5452.0000749.

Western Electric Company. 1958. *Statistical quality control handbook*. 2nd ed. New York: AT&T Technologies.

Wu, Y., and S. Liu. 2017. "A review of data-driven approaches for burst detection in water distribution systems." *Urban Water J.* 14 (9): 972–983. https://doi.org/10.1080/1573062X.2017.1279191.

Wu, Y., S. Liu, X. Wu, Y. Liu, and Y. Guan. 2016. "Burst detection in district metering areas using a data driven clustering algorithm." *Water Res.* 100: 28–37. https://doi.org/10.1016/j.watres.2016.05.016.

Ye, G., and R. A. Fenner. 2013. "Weighted least squares with expectation-maximization algorithm for burst detection in UK water distribution systems." *J. Water Resour. Plann. Manage.* 140 (4): 417–424. https://doi.org/10.1061/(ASCE)WR.1943-5452.0000344.

Zheng, Y. W., and S. Yuan. 2012. "Optimizing pressure logger placement for leakage detection and model calibration." In *Proc., 14th Water Distribution Systems Analysis Conf.*, 858–870. Barton, Australia: Engineers Australia.